IEEE Access
Multidisciplinary | Rapid Review | Open Access Journal

Received August 1, 2019, accepted August 25, 2019, date of publication September 4, 2019, date of current version October 3, 2019.

*Digital Object Identifier 10.1109/ACCESS.2019.2939480*

# Enhanced Stiffness Modeling and Identification Method for a Cable-Driven Spherical Joint Module

**KAISHENG YANG[1,2,3], GUILIN YANG[3], (Member, IEEE), SI-LU CHEN[3], YI WANG[1,3], WENJUN SHEN[1,3], TIANJIANG ZHENG[3], ZAOJUN FANG[3], AND CHONGCHONG WANG[3]**

[1]College of Materials Science and Opto-Electronic Technology, University of Chinese Academy of Sciences (UCAS), Beijing 100049, China
[2]Zhejiang Marine Development Research Institute, Zhoushan 316021, China
[3]Zhejiang Key Laboratory of Robotics and Intelligent Manufacturing Equipment Technology, Ningbo Institute of Materials Technology and Engineering, Chinese Academy of Sciences (CAS), Ningbo 315201, China

Corresponding author: Guilin Yang (glyang@nimte.ac.cn)

This work was supported in part by the National Natural Science Foundation of China under Project 51705510 and Project 51475448, in part by the NSFC-Zhejiang Joint Found for the Integration and Information under Project U1509202, in part by the Institute of robotics and Intelligent Manufacturing Innovation, Chinese Academy of Sciences, under Project C2018005, in part by the Public Welfare Technology Research Program of Zhejiang Province, China, under Project LGF19E050001, and in part by the Innovation Team of Key Components and Technology for the New Generation Robot under Grant 2016B10016.

**ABSTRACT** A cable-driven manipulator (CDM) has low stiffness and its stiffness identification is a critical issue. This paper focuses on stiffness modeling and identification for a cable-driven spherical joint module (CSJM), whose trajectory is a curve on $SO(3)$. In order to obtain the stiffness of the CSJM, it requires to evaluate the variation of the load against the displacement. However, since the vectors of displacement and load at different poses of the CSJM belong to different vector spaces of $SO(3)$, the algebraic operations between them can not be performed directly. Hence, a Riemannian metric and the Levi-Civita connection are defined on $SO(3)$, so that vectors can be parallel transported from one vector space to another along the trajectory curve. Consequently, the covariant derivative of the load with respect to the displacement is defined on $SO(3)$ to establish the stiffness model. The resultant stiffness matrix is proved to be symmetric for a conservative system. In this way, the stiffness model with the system parameters of the CSJM is derived based on the kinetostatic analysis. Due to a part of the system parameters can not be accurately known, a feasible stiffness identification method is proposed based on the approximation of the covariant derivative, which merely require to measure the poses and loads of the CSJM. The experiment on the actual testbed validates the practical appeals of the proposed stiffness model and associate identification method.

**INDEX TERMS** Cable-driven spherical joint module, stiffness modeling, stiffness identification, force/torque sensor, Riemannian manifold.

## I. INTRODUCTION

Cable-driven manipulators (CDMs) utilize lightweight cables to drive the mechanism, in which all the cable driving motors are mounted on the base [1]–[4]. As CDMs have the advantages of large workspace, high payload-to-weight ratio, low moving mass and variable stiffness, they have been applied widely in inspection and repair [5]–[7], moving and lifting payloads [8]–[10], underwater vehicles [11] and rehabilitation robots [12]–[15]. CDMs are low-stiffness systems, while their stiffness can be adjusted by controlling the cable tensions due to redundant actuation. Hence, stiffness modeling [16] and identification [17] are important issues for accurate positioning and stiffness control for CDMs, which have attracted dramatically attentions in recent years [18]. In this paper, we focus on the static stiffness modeling and identification for a cable-driven spherical joint module (CSJM), which has been designed in our prior work [19].

In the recent decades, several stiffness modeling methods have been proposed for robot manipulators. In [20], a stiffness formula for serial manipulators is proposed firstly. This formula is further extended to parallel manipulators and the

The associate editor coordinating the review of this manuscript and approving it for publication was Yingxiang Liu.

stiffness of the actuators is considered [21]. However, this formula is merely valid at the unloaded equilibrium configuration [22]. In [23], a stiffness model for a conservative mechanical system is studied and it is shown that the stiffness matrix becomes asymmetric when the system is subjected to external loads. Considering the change of the mechanism geometry under the presence of external load, the Conservative Congruence Transformation (CCT) is developed in [24], [25], which reveals the relationship of stiffness matrices between joint space and Cartesian space. Based on the CCT approach, the stiffness model of a CDM is presented in [26]. However, most of such stiffness models are studied in Euclidean space. Remarkably, the trajectory of the CSJM is a curve on $SO(3)$, which is a differential manifold [27]. The neighborhood of a point on a differential manifold can be approximated by its tangent space at this point, which is Euclidean [28]. Such approximation has been widely adopted to derive the stiffness model of a rigid manipulator with high stiffness. However, for a low stiffness system such as the CSJM, the displacement will be large under the load, which makes the former approach inaccurate. In [29], a stiffness formulation for the conservative mechanical system is derived on $SE(3)$ from geometric perspective. It shows that the stiffness matrix is dependent on the affine connection defined on $SE(3)$. In [30], a stiffness model for a wrist joint is derived on $SO(3)$ with a symmetric connection, as it yields a symmetric stiffness matrix for a conservative mechanical system. However, in this approach, the choice of a symmetric connection for a symmetric stiffness matrix is not unique. Furthermore, the symmetry of the stiffness matrix for a conservative mechanical system has not been strictly proved.

Stiffness identification is a complex task for robotic systems since only a subset of system state variables can be measured and the linear regressions can not be employed directly [31]. In the last decades, the stiffness identification of rigid robots has been widely investigated, and several approaches have been proposed [32]–[34]. The common approach is based on the inverse dynamic model and the least squares estimation to identify inertial parameters of robot manipulators [35]–[38]. Another approach is called closed-loop output error method which needs to simulate the robot controllers [39], [40]. Such an approach requires the internal data of the robots, such as motor torques or controller outputs, which are hard to be measured. In order to overcome this problem, an external measurement approach is considered, in which a force/torque sensor is fixed on the end-effector of the manipulator to measure the loads and a high precision Cartesian position sensor is employed to measure the associate end-effector's pose [33], [41]. In this way, all factors related to the pose variation of the end-effector, such as deformations on cables, links, joints, and cable driving motors, are reflected in the coming stiffness model. However, a systematic stiffness identification approach on a non-Euclidean space is not well studied, which is applicable for the case when a loaded end-effector encounters large variation of its pose.

In this paper, we focus on the development of a more accurate stiffness model and its associate identification method for a CSJM. The motion trajectory of the CSJM is a curve on $SO(3)$, which is a non-Euclidean space. As a low stiffness mechanical system, the CSJM encounters large variation of its pose under the load. However, the vectors of displacement and load at different poses of the CSJM belong to different vector spaces, which are tangent or cotangent spaces of $SO(3)$, so we can not perform algebraic operations between them directly to establish the stiffness model. To solve this problem, a Riemannian metric is defined on $SO(3)$ to evaluate the lengths of vectors and the angles between vectors, and an affine connection called Levi-Civita connection is introduced to bridge different vector spaces of $SO(3)$. In this way, the stiffness of the CSJM is derived from the covariant derivative of the load with respect to the displacement. In addition, it is proved that the derived stiffness matrix is symmetric for a conservative system. In order to reveal the relationship between the stiffness and the system parameters of the CSJM, the stiffness model is developed based on the kinetostatic analysis of the CSJM. It shows that the stiffness of the CSJM is determined by the pose of the module, the cable tensions, the stiffness of the cables and associate driving units. Since the later two sets of parameters are difficult to measure accurately, a stiffness identification method based on the approximation of this covariant derivative is developed, which only requires to measure sets of loads and associate displacements of the CSJM. The experiment on the actual testbed validates the effectiveness of the proposed method.

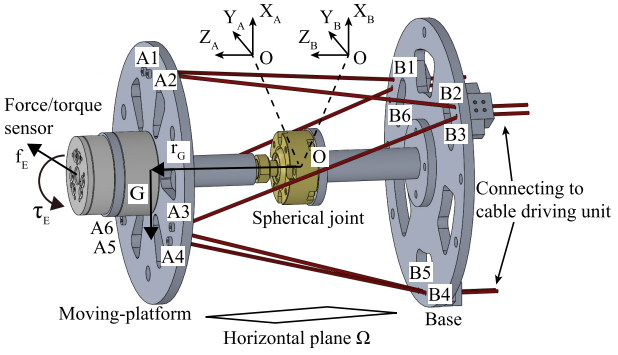


**FIGURE 1.** CAD model of CSJM.

## II. STIFFNESS MODEL OF CSJM

As shown in Figure 1, the CSJM is made up of a moving-platform, a base, a passive spherical joint, cables and cable driving units. In this design, six cables are employed to maximize the workspace [42]. There are six small holes on both of the moving-platform and the base for cables mounting or passing through, denoted by $A_i$ $(i = 1, 2, \cdots, 6)$ and $B_j$ $(j = 1, 2, \cdots, 6)$, respectively. Due to the symmetric design, $A_2\,A_3 = A_4\,A_5 = A_6\,A_1$, $B_1\,B_2 = B_3\,B_4 = B_5\,B_6$, $A_1\,A_2 = A_3\,A_4 = A_5\,A_6$ and $B_2\,B_3 = B_4\,B_5 = B_6\,B_1$. $O$, $O_A$ and $O_B$ are the centers of the passive spherical joint,

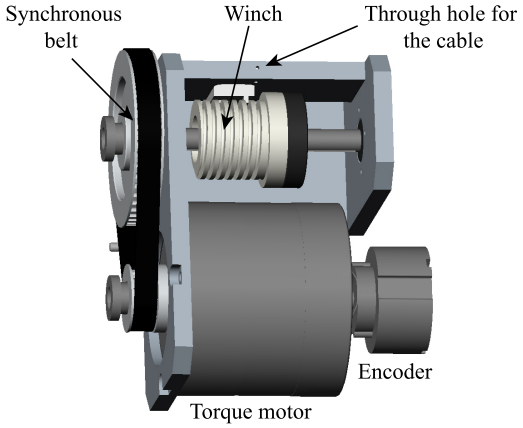


**FIGURE 2.** CAD model of cable driving unit.

moving-platform and base, respectively. A 6-axis force/torque sensor is fixed at the top of the moving-platform for the measurement of external loads. The cables are actuated by the cable driving units, as shown in Figure 2.

In order to describe the motion of the CSJM, a coordinate frame is attached to the base, called base frame {B}, and another frame is attached to the moving-platform, called moving frame {A}. In this way, the motion of the CSJM can be represented by the moving frame {A} with respect to the base frame {B}. As the stiffness of the CSJM is related with the displacements and the applied loads, we will study the kinetostatics analysis of the CSJM by differential geometric theory, which will eventually lead to a modified stiffness model.

### A. TANGENT SPACE ON SO(3)

The moving-platform of the CSJM rotates with respect to the spherical joint and the rotation motion can be represented by a rotation matrix $\boldsymbol{R} \in SO(3)$. Thus, the trajectory of the CSJM is a parameterized curve with respect to time, such that $\boldsymbol{R}(t) \in SO(3)$ for $t > 0$. According to the exponential map of the rotation matrix [27], the curve $\boldsymbol{R}(t) \in SO(3)$ is represented by the following expression

$$\boldsymbol{R}(t) = e^{\hat{\boldsymbol{\xi}}(t)}, \tag{1}$$

where $\hat{\boldsymbol{\xi}}(t) \in so(3)$ and $\boldsymbol{\xi}(t) = (\xi_1, \xi_2, \xi_3)^T \in \mathbb{R}^3$ is called canonical coordinates with respect to the basis of $so(3)$ [27]. Here, $\boldsymbol{\xi}$ and $\hat{\boldsymbol{\xi}}$ satisfy

$$\boldsymbol{\xi} = \begin{pmatrix} \xi_1 \\ \xi_2 \\ \xi_3 \end{pmatrix} \rightarrow \hat{\boldsymbol{\xi}} = \begin{pmatrix} 0 & -\xi_3 & \xi_2 \\ \xi_3 & 0 & -\xi_1 \\ -\xi_2 & \xi_1 & 0 \end{pmatrix}. \tag{2}$$

The derivative of $\boldsymbol{R}(t)$ with respect to the parameter $t$, denoted as $\dot{\boldsymbol{R}}(t)$, belongs to the tangent space of $SO(3)$ at the point $\boldsymbol{R}(t)$, denoted as $T_{\boldsymbol{R}(t)}SO(3)$. Elements of the tangent space are called tangent vectors. The tangent vector $\dot{\boldsymbol{R}}(t)$ represents the velocity of the CSJM and satisfies the following expression

$$\dot{\boldsymbol{R}}(t) = \boldsymbol{R}(t)\hat{\boldsymbol{\omega}}(t), \tag{3}$$

where $\boldsymbol{\omega}(t) = \dot{\boldsymbol{\xi}}(t) \in \mathbb{R}^3$ is called the body velocity of the CSJM and $\hat{\boldsymbol{\omega}}(t)$ is an element of $so(3)$.

Let $\hat{\boldsymbol{\sigma}}_i$ $(i = 1, 2, 3)$ be the standard basis for $so(3)$, where $\boldsymbol{\sigma}_1 = (1, 0, 0)^T$, $\boldsymbol{\sigma}_2 = (0, 1, 0)^T$ and $\boldsymbol{\sigma}_3 = (0, 0, 1)^T$, then $\hat{\boldsymbol{\omega}} \in so(3)$ can be represented as following

$$\hat{\boldsymbol{\omega}} = \sum_{i=1}^{3} \omega^i \hat{\boldsymbol{\sigma}}_i, \tag{4}$$

where $\omega^i$ $(i = 1, 2, 3)$ is the coordinate of $\hat{\boldsymbol{\omega}}$ with respect to the basis $\hat{\boldsymbol{\sigma}}_i$ $(i = 1, 2, 3)$. Thus, the tangent vector $\dot{\boldsymbol{R}}(t)$ can be expressed as following

$$\dot{\boldsymbol{R}}(t) = \boldsymbol{R}(t)\sum_{i=1}^{3} \omega^i \hat{\boldsymbol{\sigma}}_i = \sum_{i=1}^{3} \omega^i \boldsymbol{R}(t)\hat{\boldsymbol{\sigma}}_i = \sum_{i=1}^{3} \omega^i \boldsymbol{L}_i|_{\boldsymbol{R}(t)}, \tag{5}$$

where $\boldsymbol{L}_i|_{\boldsymbol{R}(t)} = \boldsymbol{R}(t)\hat{\boldsymbol{\sigma}}_i$ $(i = 1, 2, 3)$ is the standard basis for $T_{\boldsymbol{R}(t)}SO(3)$. Sometimes we write $\boldsymbol{L}_i|_{\boldsymbol{R}(t)}$ as $\boldsymbol{L}_i$ for simplification. Comparing (4) and (5), the coordinate of $\dot{\boldsymbol{R}}(t)$ equals to that of $\hat{\boldsymbol{\omega}}$, which shows that $T_{\boldsymbol{R}(t)}SO(3)$ is isomorphic to $so(3)$.

For a given $\boldsymbol{U} \in SO(3)$, the transformation $\boldsymbol{U}\boldsymbol{R}(t)$ is called a left translation of $\boldsymbol{R}(t)$ by $\boldsymbol{U}$, and the transformation $\boldsymbol{R}(t)\boldsymbol{U}$ is called a right translation of $\boldsymbol{R}(t)$ by $\boldsymbol{U}$. Let $\boldsymbol{Q}(t) = \boldsymbol{U}\boldsymbol{R}(t) \in SO(3)$ be a left translation of $\boldsymbol{R}(t)$, the tangent vector $\dot{\boldsymbol{Q}}(t) \in T_{\boldsymbol{Q}(t)}SO(3)$ satisfies

$$\begin{aligned} \dot{\boldsymbol{Q}}(t) &= \boldsymbol{U}\dot{\boldsymbol{R}}(t) = \boldsymbol{U}\sum_{i=1}^{3} \omega^i \boldsymbol{L}_i|_{\boldsymbol{R}(t)} \\ &= \sum_{i=1}^{3} \omega^i \boldsymbol{U}\boldsymbol{L}_i|_{\boldsymbol{R}(t)} = \sum_{i=1}^{3} \omega^i \boldsymbol{L}_i|_{\boldsymbol{Q}(t)}. \end{aligned} \tag{6}$$

It shows that, with respect to the basis $\boldsymbol{L}_i$ $(i = 1, 2, 3)$, the coordinate of the tangent vector $\dot{\boldsymbol{Q}}(t)$ equals to that of the tangent vector $\dot{\boldsymbol{R}}(t)$, both of which are $\omega^i$ $(i = 1, 2, 3)$. Then $T_{\boldsymbol{R}(t)}SO(3)$ is called a left invariant vector field on $SO(3)$ and $\boldsymbol{L}_i$ $(i = 1, 2, 3)$ is the basis of left invariant vector field.

In order to evaluate the length of a vector and the angle between two nonzero vectors in $T_{\boldsymbol{R}(t)}SO(3)$, an inner product is defined. For $\boldsymbol{X}, \boldsymbol{Y} \in T_{\boldsymbol{R}(t)}SO(3)$, where $\boldsymbol{X} = \sum_{i=1}^{3} X^i \boldsymbol{L}_i$ $(i = 1, 2, 3)$ and $\boldsymbol{Y} = \sum_{j=1}^{3} Y^j \boldsymbol{L}_j$ $(j = 1, 2, 3)$, the inner product of $\boldsymbol{X}$ and $\boldsymbol{Y}$, $\langle \boldsymbol{X}, \boldsymbol{Y} \rangle$, is defined as

$$\langle \boldsymbol{X}, \boldsymbol{Y} \rangle = \sum_{i=1}^{3}\sum_{j=1}^{3} g_{ij} X^i Y^j, \tag{7}$$

where $\boldsymbol{g} = \{g_{ij}\} \in \mathbb{R}^{3\times 3}$ is a symmetric and positive definite matrix, called Riemannian metric on $SO(3)$. Equipped with a Riemannian metric, $SO(3)$ becomes a Riemannian manifold. Consequently, the length or norm of a vector $\boldsymbol{X} \in T_{\boldsymbol{R}(t)}SO(3)$ is defined as

$$|\boldsymbol{X}| = \langle \boldsymbol{X}, \boldsymbol{X} \rangle^{\frac{1}{2}}, \tag{8}$$

and the angle between two nonzero vectors $\boldsymbol{X}, \boldsymbol{Y} \in T_{\boldsymbol{R}(t)}SO(3)$ is defined by an unique $\theta \in [0, \pi]$ satisfying

$$\cos\theta = \frac{\langle \boldsymbol{X}, \boldsymbol{Y}\rangle}{|\boldsymbol{X}||\boldsymbol{Y}|}. \tag{9}$$

To describe the motion of the CSJM, it is necessary to preserve the length of a vector and the angle between two vectors in the tangent space under the left translations along $\boldsymbol{R}(t)$, i.e., $\langle \boldsymbol{UX}, \boldsymbol{UY}\rangle = \langle \boldsymbol{X}, \boldsymbol{Y}\rangle$ yields for all $\boldsymbol{U} \in SO(3)$. Then $\boldsymbol{g} = \alpha \boldsymbol{I}_{3\times 3}$ is required, where $\alpha \in \mathbb{R}$ depends on the choice of scale [27]. Here $\alpha = 1$ is chosen, which leads

$$\langle \boldsymbol{X}, \boldsymbol{Y}\rangle = \sum_{i=1}^{3} X^i Y^i. \tag{10}$$

The metric matrix $\boldsymbol{g}$ is called left invariant, as it preserves the inner product on $T_{\boldsymbol{R}(t)}SO(3)$ under left translations along $\boldsymbol{R}(t)$.

On the other hand, since $\boldsymbol{\omega}(t)$ is the body velocity of the CSJM, then $\boldsymbol{\omega}_s(t) = \boldsymbol{R}(t)\boldsymbol{\omega}(t) \in \mathbb{R}^3$ is the spatial velocity of the CSJM. The corresponding twist $\hat{\boldsymbol{\omega}}_s(t) \in so(3)$ satisfies

$$\hat{\boldsymbol{\omega}}_s(t) = \boldsymbol{R}(t)\hat{\boldsymbol{\omega}}(t)\boldsymbol{R}(t)^{-1}. \tag{11}$$

Substituting (11) into (3), we have

$$\dot{\boldsymbol{R}}(t) = \boldsymbol{R}(t)\hat{\boldsymbol{\omega}}(t) = \hat{\boldsymbol{\omega}}_s(t)\boldsymbol{R}(t). \tag{12}$$

It shows that the tangent vector $\dot{\boldsymbol{R}}(t)$ is not only a left translation of the twist $\hat{\boldsymbol{\omega}}(t)$ by $\boldsymbol{R}(t)$ but also a right translation of the twist $\hat{\boldsymbol{\omega}}_s(t)$ by $\boldsymbol{R}(t)$. Similarly, it can be concluded that $T_{\boldsymbol{R}(t)}SO(3)$ is also a right invariant vector field on $SO(3)$ and $\boldsymbol{g}$ is also right invariant. Thus, $T_{\boldsymbol{R}(t)}SO(3)$ and $\boldsymbol{g}$ are called bi-invariant, as they are both left invariant and right invariant.

### B. COTANGENT SPACE ON SO(3)

For the CSJM, the body velocity $\hat{\boldsymbol{\omega}}$ is a twist which belongs to $so(3)$ and the moment load $\hat{\boldsymbol{\tau}}$ is a wrench which belongs to $so^*(3)$, the dual space of $so(3)$ [27]. Let $\hat{\boldsymbol{\lambda}}^j$ $(j = 1, 2, 3)$ be the basis for $so^*(3)$, which is the dual basis for $so(3)$ (i.e.,$\hat{\boldsymbol{\sigma}}_i$ $(i = 1, 2, 3)$), then $\hat{\boldsymbol{\tau}}$ yields

$$\hat{\boldsymbol{\tau}} = \sum_{j=1}^{3} \tau_j \hat{\boldsymbol{\lambda}}^j, \tag{13}$$

where $\tau_j$ $(j = 1, 2, 3)$ is the coordinate of $\hat{\boldsymbol{\tau}}$ with respect to the basis $\hat{\boldsymbol{\lambda}}^j$ $(j = 1, 2, 3)$. The tangent vector $\dot{\boldsymbol{R}}(t) \in T_{\boldsymbol{R}(t)}SO(3)$ represents the velocity of the CSJM, and $T_{\boldsymbol{R}(t)}SO(3)$ is isomorphic to $so(3)$. By analogy with the tangent vector, we define

$$\boldsymbol{F}(t) = \boldsymbol{R}(t)\hat{\boldsymbol{\tau}}(t) = \sum_{j=1}^{3} \tau_j \boldsymbol{R}(t)\hat{\boldsymbol{\lambda}}^j = \sum_{j=1}^{3} \tau_i \boldsymbol{\Lambda}^j|_{\boldsymbol{R}(t)}, \tag{14}$$

where $\boldsymbol{\Lambda}^j|_{\boldsymbol{R}(t)} = \boldsymbol{R}(t)\hat{\boldsymbol{\lambda}}^j$ $(j = 1, 2, 3)$. $\boldsymbol{F}(t)$ belongs to the dual space of the tangent space at $\boldsymbol{R}(t)$, called cotangent space $T^*_{\boldsymbol{R}(t)}SO(3)$. $T^*_{\boldsymbol{R}(t)}SO(3)$ is a real-value linear functional on $T_{\boldsymbol{R}(t)}SO(3)$ [43]. The elements of a cotangent space are termed as cotangent vectors, or one-forms. $\boldsymbol{\Lambda}^j$ $(j = 1, 2, 3)$ is the basis for $T^*_{\boldsymbol{R}(t)}SO(3)$, which is the dual basis for $T_{\boldsymbol{R}(t)}SO(3)$ (i.e., $\boldsymbol{L}_i$ $(i = 1, 2, 3)$) and it yields

$$\langle \boldsymbol{L}_i, \boldsymbol{\Lambda}^j\rangle = \delta_i^j = \begin{cases} 1 & (i = j) \\ 0 & (i \neq j) \end{cases} \quad (i, j = 1, 2, 3). \tag{15}$$

Similarly, with the basis $\boldsymbol{\Lambda}^j$ $(j = 1, 2, 3)$, $T^*_{\boldsymbol{R}(t)}SO(3)$ is isomorphic to $so^*(3)$ and the cotangent vector $\boldsymbol{F}(t)$ represents the load applied on the CSJM. Furthermore, $T^*_{\boldsymbol{R}(t)}SO(3)$ is also a bi-invariant vector field.

### C. DIFFERENTIAL FORM ON SO(3)

Conventionally, the stiffness of a robotic manipulator is modeled as the derivative of the applied load with respect to the displacement in Euclidean space. However, as a low stiffness system, the displacements and loads at different poses of the CSJM belong to different tangent spaces and cotangent spaces on $SO(3)$, respectively. They can not perform algebraic operation directly. To solve this problem, an affine connection is introduced on $SO(3)$, which bridges any two vector spaces on $SO(3)$. It provides a notation of parallel transport that specifies how to transport a vector from one vector space to another along a curve on $SO(3)$ in parallel [44].

Given a parallel transport $\boldsymbol{P}_{t,t_0}^{\boldsymbol{R}(t)} : T_{\boldsymbol{R}(t)}SO(3) \to T_{\boldsymbol{R}(t_0)}SO(3)$, it transports a vector in $T_{\boldsymbol{R}(t)}SO(3)$ to the vector in $T_{\boldsymbol{R}(t_0)}SO(3)$ along $\boldsymbol{R}(t)$ on $SO(3)$. $\boldsymbol{P}_{t,t_0}^{\boldsymbol{R}(t)}(\boldsymbol{X}(t))$ represents the parallel transport of the vector $\boldsymbol{X}(t) \in T_{\boldsymbol{R}(t)}SO(3)$ along $\boldsymbol{R}(t)$ back to $T_{\boldsymbol{R}(t_0)}SO(3)$. Based on the parallel transport, the covariant derivative is defined on $SO(3)$ as

$$\nabla_{\dot{\boldsymbol{R}}}\boldsymbol{X}\big|_{\boldsymbol{R}(t_0)} = \lim_{t\to t_0} \frac{\boldsymbol{P}_{t,t_0}^{\boldsymbol{R}(t)}(\boldsymbol{X}(t)) - \boldsymbol{X}(t_0)}{t - t_0}. \tag{16}$$

where $\nabla_{\dot{\boldsymbol{R}}}\boldsymbol{X}\big|_{\boldsymbol{R}(t_0)}$ is the covariant derivative of the vector $\boldsymbol{X}$ at $\boldsymbol{R}(t_0)$ along $\dot{\boldsymbol{R}}(t)$.

Furthermore, denoting $\mathscr{T}(SO(3))$ as the collection of all vector spaces on $SO(3)$, for $\boldsymbol{X}, \boldsymbol{Y} \in \mathscr{T}(SO(3))$, $\nabla_{\boldsymbol{Y}}\boldsymbol{X}$ represents the covariant derivative of $\boldsymbol{X}$ in the direction $\boldsymbol{Y}$. Given $\boldsymbol{X}, \boldsymbol{Y}, \boldsymbol{Z} \in \mathscr{T}(SO(3))$ and $\alpha, \beta \in \mathbb{R}$, the covariant derivative satisfies the following rules

$$\nabla_{\alpha\boldsymbol{X}+\beta\boldsymbol{Y}}\boldsymbol{Z} = \alpha\nabla_{\boldsymbol{X}}\boldsymbol{Z} + \beta\nabla_{\boldsymbol{Y}}\boldsymbol{Z}, \tag{17a}$$

$$\nabla_{\boldsymbol{Z}}(\alpha\boldsymbol{X} + \beta\boldsymbol{Y}) = \alpha\nabla_{\boldsymbol{Z}}\boldsymbol{X} + \beta\nabla_{\boldsymbol{Z}}\boldsymbol{Y}. \tag{17b}$$

For a real-valued function $f$ on $SO(3)$, such as the potential energy of the CSJM, $\nabla_{\boldsymbol{Z}}f$ represents the derivative of $f$ in direction $\boldsymbol{Z}$, usually written as $\boldsymbol{Z} \circ f$.

Since $T_{\boldsymbol{R}(t)}SO(3)$ is bi-invariant, which means the components of $\dot{\boldsymbol{R}}(t) \in T_{\boldsymbol{R}(t)}SO(3)$, $\omega^i$ $(i = 1, 2, 3)$, are constant under left and right translations along $\boldsymbol{R}(t)$, the parallel transport of $\dot{\boldsymbol{R}}(t)$ satisfies $\boldsymbol{P}_{t,t_0}^{\boldsymbol{R}(t)}(\dot{\boldsymbol{R}}(t)) \equiv \dot{\boldsymbol{R}}(t_0)$. Thus, according to (16), the covariant derivative of $\dot{\boldsymbol{R}}(t)$ along $\boldsymbol{R}(t)$ satisfies

$$\nabla_{\dot{\boldsymbol{R}}}\dot{\boldsymbol{R}} \equiv 0. \tag{18}$$

The curve $\boldsymbol{R}(t)$ which satisfies (18) is called a geodesic on $SO(3)$ [43]. Particularly, the geodesics in Euclidean space are straight lines.

There exist many affine connections on $SO(3)$, which lead to various parallel transports and the associate covariant derivatives. Here, we require a particular affine connection that reflects the properties of the motion of the CSJM:

- $T_{\boldsymbol{R}(t)}SO(3)$ and $\boldsymbol{g}$ are bi-invariant.
- $\boldsymbol{R}(t)$ is a geodesic on $SO(3)$ with respect to the chosen affine connection.

An affine connection on $SO(3)$, called the Levi-Civita connection, yields the above conditions. Given $\boldsymbol{X}, \boldsymbol{Y}, \boldsymbol{Z} \in \mathscr{T}(SO(3))$, the Levi-Civita connection is specified by the following properties

- Symmetry:

$$\nabla_{\boldsymbol{X}}\boldsymbol{Y} - \nabla_{\boldsymbol{Y}}\boldsymbol{X} - [\boldsymbol{X}, \boldsymbol{Y}] = 0, \tag{19}$$

- Compatibility with the metric $\boldsymbol{g}$:

$$\boldsymbol{Z} \circ \langle \boldsymbol{X}, \boldsymbol{Y} \rangle = \langle \nabla_{\boldsymbol{Z}}\boldsymbol{X}, \boldsymbol{Y} \rangle + \langle \boldsymbol{X}, \nabla_{\boldsymbol{Z}}\boldsymbol{Y} \rangle, \tag{20}$$

where $[\boldsymbol{X}, \boldsymbol{Y}]$ represents the Lie bracket of vectors $\boldsymbol{X}$ and $\boldsymbol{Y}$, and $\boldsymbol{Z} \circ \langle \boldsymbol{X}, \boldsymbol{Y} \rangle$ represents the derivative of a real-valued function $\langle \boldsymbol{X}, \boldsymbol{Y} \rangle$ in direction $\boldsymbol{Z}$. Eventually, $SO(3)$ is endowed with metric $\boldsymbol{g}$ and the associate Levi-Civita connection [43].

### D. STIFFNESS MODEL ON SO(3)

Let $\boldsymbol{V}(t) = \dot{\boldsymbol{R}}(t) \in \mathbb{R}^3$, then $\boldsymbol{V}\delta t$ represents the instantaneous displacement of the CSJM. The covariant derivative of the load with respect to the displacement is given by $\nabla_{\boldsymbol{V}\delta t}\boldsymbol{F}$. According to (17a), $\nabla_{\boldsymbol{V}\delta t}\boldsymbol{F}$ satisfies the following equation

$$\begin{aligned} \nabla_{\boldsymbol{V}\delta t}\boldsymbol{F} &= \delta t \nabla_{\sum_{i=1}^{3}\omega^i \boldsymbol{L}_i}\boldsymbol{F} \\ &= \delta t \sum_{i=1}^{3} \omega^i \nabla_{\boldsymbol{L}_i}\boldsymbol{F} = \delta t \boldsymbol{K}\boldsymbol{\omega} = \boldsymbol{K}\delta\boldsymbol{\zeta}. \end{aligned} \tag{21}$$

where $\boldsymbol{K} = (\nabla_{\boldsymbol{L}_1}\boldsymbol{F}, \nabla_{\boldsymbol{L}_2}\boldsymbol{F}, \nabla_{\boldsymbol{L}_3}\boldsymbol{F}) \in \mathbb{R}^{3\times 3}$ represents the stiffness of the CSJM. The components of $\boldsymbol{K}$, $K_{ij}$ $(i, j = 1, 2, 3)$, yield the following expression

$$K_{ij} = \langle \nabla_{\boldsymbol{L}_j}\boldsymbol{F}, \boldsymbol{L}_i \rangle. \tag{22}$$

According to (20), we have

$$\boldsymbol{L}_j \circ \langle \boldsymbol{F}, \boldsymbol{L}_i \rangle = \langle \nabla_{\boldsymbol{L}_j}\boldsymbol{F}, \boldsymbol{L}_i \rangle + \langle \boldsymbol{F}, \nabla_{\boldsymbol{L}_j}\boldsymbol{L}_i \rangle. \tag{23}$$

So, the components of the stiffness yield

$$K_{ij} = \boldsymbol{L}_j \circ \langle \boldsymbol{F}, \boldsymbol{L}_i \rangle - \langle \boldsymbol{F}, \nabla_{\boldsymbol{L}_j}\boldsymbol{L}_i \rangle. \tag{24}$$

Since $\boldsymbol{R}(t)$ is a geodesic on $SO(3)$, it yields $\nabla_{\dot{\boldsymbol{R}}}\dot{\boldsymbol{R}} \equiv 0$. On the other hand, the coordinate of $\dot{\boldsymbol{R}}(t)$, $\omega^j$ $(j = 1, 2, 3)$, is constant under the left translations along $\boldsymbol{R}(t)$, so we have the following equation via (17), i.e.,

$$\begin{aligned} \nabla_{\dot{\boldsymbol{R}}}\dot{\boldsymbol{R}} &= \nabla_{\sum_{i=1}^{3}\omega^i \boldsymbol{L}_i} \sum_{i=j}^{3} \omega^j \boldsymbol{L}_j \\ &= \sum_{i=1}^{3}\sum_{j=1}^{3} \omega^i \omega^j \nabla_{\boldsymbol{L}_i}\boldsymbol{L}_j \equiv 0. \end{aligned} \tag{25}$$

It holds for any $(\omega^1, \omega^2, \omega^3)$ if and only if

$$\nabla_{\boldsymbol{L}_i}\boldsymbol{L}_j + \nabla_{\boldsymbol{L}_j}\boldsymbol{L}_i = 0. \tag{26}$$

According to (19), we have

$$\nabla_{\boldsymbol{L}_j}\boldsymbol{L}_i - \nabla_{\boldsymbol{L}_i}\boldsymbol{L}_j = [\boldsymbol{L}_j, \boldsymbol{L}_i]. \tag{27}$$

Additionally, it can be concluded via (26) and (27)

$$\nabla_{\boldsymbol{L}_j}\boldsymbol{L}_i = \frac{1}{2}[\boldsymbol{L}_j, \boldsymbol{L}_i]. \tag{28}$$

According to the property of the Lie bracket [43], it yields

$$[\boldsymbol{L}_j, \boldsymbol{L}_i] = [\boldsymbol{R}\hat{\boldsymbol{\sigma}}_j, \boldsymbol{R}\hat{\boldsymbol{\sigma}}_i] = \boldsymbol{R}[\hat{\boldsymbol{\sigma}}_j, \hat{\boldsymbol{\sigma}}_i]. \tag{29}$$

Since $[\hat{\boldsymbol{\sigma}}_j, \hat{\boldsymbol{\sigma}}_i] = \hat{\boldsymbol{\sigma}}_j\hat{\boldsymbol{\sigma}}_i - \hat{\boldsymbol{\sigma}}_i\hat{\boldsymbol{\sigma}}_j$, it can also be represented by the following expression

$$[\hat{\boldsymbol{\sigma}}_j, \hat{\boldsymbol{\sigma}}_i] = \sum_{k=1}^{3} \gamma_{ji}^k \hat{\boldsymbol{\sigma}}_k, \tag{30}$$

where the coefficients $\gamma_{ji}^k$ $(i, j, k = 1, 2, 3) \in \mathbb{R}$ are zero except

$$\gamma_{12}^3 = \gamma_{31}^2 = \gamma_{23}^1 = 2, \tag{31a}$$

$$\gamma_{21}^3 = \gamma_{13}^2 = \gamma_{32}^1 = -2. \tag{31b}$$

Since $\boldsymbol{g}$ is left invariant, it yields

$$\langle \boldsymbol{F}, \boldsymbol{L}_i \rangle = \langle \boldsymbol{\tau}, \boldsymbol{\sigma}_i \rangle = \tau_i, \tag{32a}$$

$$\begin{aligned} \langle \boldsymbol{F}, \nabla_{\boldsymbol{L}_j}\boldsymbol{L}_i \rangle &= \langle \boldsymbol{F}, \frac{1}{2}[\boldsymbol{L}_j, \boldsymbol{L}_i] \rangle = \langle \boldsymbol{\tau}, \frac{1}{2}[\hat{\boldsymbol{\sigma}}_j, \hat{\boldsymbol{\sigma}}_i] \rangle \\ &= \frac{1}{2}\sum_{k=1}^{3} \tau_k \gamma_{ji}^k. \end{aligned} \tag{32b}$$

Thus, the components of the stiffness matrix $\boldsymbol{K}$ can be given as following

$$\begin{aligned} K_{ij} &= \boldsymbol{L}_j \circ \langle \boldsymbol{F}, \boldsymbol{L}_i \rangle - \langle \boldsymbol{F}, \nabla_{\boldsymbol{L}_j}\boldsymbol{L}_i \rangle \\ &= \boldsymbol{L}_j \circ \tau_i - \frac{1}{2}\sum_{k=1}^{3} \tau_k \gamma_{ji}^k. \end{aligned} \tag{33}$$

The CSJM is a conservative mechanical system if the friction is neglected. Denote the potential energy of the module as $\Phi$, its derivative along a specific direction equals the work done by a one-form $\boldsymbol{F}$ against this direction [30], i.e.,

$$\boldsymbol{L}_i \circ \Phi = -\langle \boldsymbol{F}, \boldsymbol{L}_i \rangle = -\tau_i. \tag{34}$$

In order to evaluate the symmetry of the stiffness matrix, we compute the following expression

$$\begin{aligned} K_{ij} - K_{ji} &= (\boldsymbol{L}_j \circ \langle \boldsymbol{F}, \boldsymbol{L}_i \rangle - \langle \boldsymbol{F}, \nabla_{\boldsymbol{L}_j}\boldsymbol{L}_i \rangle) \\ &\quad - (\boldsymbol{L}_i \circ \langle \boldsymbol{F}, \boldsymbol{L}_j \rangle - \langle \boldsymbol{F}, \nabla_{\boldsymbol{L}_i}\boldsymbol{L}_j \rangle) \\ &= (\boldsymbol{L}_i \circ (\boldsymbol{L}_j \circ \Phi) - \boldsymbol{L}_j \circ (\boldsymbol{L}_i \circ \Phi)) \\ &\quad + (\langle \boldsymbol{F}, \nabla_{\boldsymbol{L}_i}\boldsymbol{L}_j \rangle - \langle \boldsymbol{F}, \nabla_{\boldsymbol{L}_j}\boldsymbol{L}_i \rangle). \end{aligned} \tag{35}$$

According to the property of the Lie bracket [43], it yields

$$\begin{aligned} \boldsymbol{L}_i \circ (\boldsymbol{L}_j \circ \Phi) - \boldsymbol{L}_j \circ (\boldsymbol{L}_i \circ \Phi) &= [\boldsymbol{L}_i, \boldsymbol{L}_j] \circ \Phi \\ &= -\langle \boldsymbol{F}, [\boldsymbol{L}_i, \boldsymbol{L}_j] \rangle. \end{aligned} \tag{36}$$

Substituting (28) and (36) into (35), we have

$$K_{ij} - K_{ji} = -\langle \boldsymbol{F}, [\boldsymbol{L}_i, \boldsymbol{L}_j] \rangle + 2\langle \boldsymbol{F}, \frac{1}{2}[\boldsymbol{L}_i, \boldsymbol{L}_j] \rangle = 0. \quad (37)$$

It shows that, as a conservative mechanical system, the stiffness matrix $\boldsymbol{K}$ of the CSJM is symmetric at every pose, regardless of the external load applied on the CSJM.

### E. STIFFNESS MODEL OF CSJM WITH SYSTEM PARAMETERS

The stiffness model shown in (33) is given by the load and displacement of the CSJM. In order to reveal the relationship of the stiffness matrix and the system parameters of the CSJM, we will derive the stiffness model with the system parameters in this section.

As shown in Figure 1, denote $\boldsymbol{a}_i = \overrightarrow{OA_i}$ and $\boldsymbol{b}_i = \overrightarrow{OB_i}$ $(i = 1, 2, \cdots, 6)$ as the position vector of points $A_i$ and $B_i$, respectively, then $\boldsymbol{c}_i = \boldsymbol{b}_i - \boldsymbol{a}_i = c_i \boldsymbol{u}_i$ represents the $i^{th}$ cable vector, where $c_i = \|\boldsymbol{c}_i\|$ is the length of the cable and $\boldsymbol{u}_i = \boldsymbol{c}_i / c_i$ is the unitary vector of $\boldsymbol{c}_i$. Denote $\boldsymbol{\tau}$ as the moment acted on the moving-platform with respect to the center $O$ and $\boldsymbol{t}_i = t_i \boldsymbol{u}_i$ as the cable tension vector of the $i^{th}$ cable, where $t_i = \|\boldsymbol{t}_i\|$, the equilibrium equation of the moving-platform is given below

$$\boldsymbol{\tau} = \sum_{i=1}^{6} \boldsymbol{a}_i \times \boldsymbol{t}_i = \sum_{i=1}^{6} (\boldsymbol{a}_i \times \boldsymbol{u}_i) t_i = \boldsymbol{J}^T \boldsymbol{T}, \quad (38)$$

where $\boldsymbol{T} = (t_1, t_2, \cdots, t_6)^T \in \mathbb{R}^{6\times 1}$ represents the vector of the six cable tensions and $\boldsymbol{J} = (\boldsymbol{a}_1 \times \boldsymbol{u}_1, \boldsymbol{a}_2 \times \boldsymbol{u}_2, \cdots, \boldsymbol{a}_6 \times \boldsymbol{u}_6)^T \in \mathbb{R}^{6\times 3}$ represents the Jacobian.

Denote $\boldsymbol{C} = (c_1, c_2, \cdots, c_6)^T$ as the vector of the six cable lengths, according to the principle of virtual work, it yields

$$-\boldsymbol{T}^T \delta \boldsymbol{C} = \boldsymbol{\tau}^T \delta \boldsymbol{\zeta}, \quad (39)$$

Substituting (38) into (39), we have

$$\delta \boldsymbol{C} = -\boldsymbol{J} \delta \boldsymbol{\zeta}, \quad (40)$$

Denote $J_{si}$ $(s = 1, 2, \cdots, 6; i = 1, 2, 3)$ as the components of Jacobian $\boldsymbol{J}$, according to (38), the components of $\boldsymbol{\tau}$ yields

$$\tau_i = \sum_{s=1}^{6} J_{si} t_s. \quad (41)$$

Then $\boldsymbol{L}_j \circ \tau_i$ can be represented by

$$\begin{aligned} \boldsymbol{L}_j \circ \tau_i &= \lim_{\Delta t \to 0} \frac{\tau_i\big|_{\boldsymbol{R}(t+\Delta t)} - \tau_i\big|_{\boldsymbol{R}(t)}}{\omega^j \Delta t} \\ &= \frac{\partial \tau_i}{\partial \zeta^j}\bigg|_{\boldsymbol{R}(t)} \\ &= \sum_{s=1}^{6} \left( \frac{\partial J_{si}}{\partial \zeta^j} t_s + J_{si} \frac{\partial t_s}{\partial \zeta^j} \right). \end{aligned} \quad (42)$$

where $\tau_i\big|_{\boldsymbol{R}(t)}$ represents the component of the moment $\boldsymbol{\tau}$ at the pose $\boldsymbol{R}(t)$. Since $\frac{\partial c_s}{\partial \zeta^j} = -J_{sj}$, according to (40), we have

$$\frac{\partial t_s}{\partial \zeta^j} = \frac{\partial t_s}{\partial c_s} \frac{\partial c_s}{\partial \zeta^j} = -k_s J_{sj}. \quad (43)$$

where $k_s = \frac{\partial t_s}{\partial c_s}$ represents the stiffness of the $s^{th}$ cable with its cable driving unit. Substituting (41), (42) and (43) into the model (33), the component of the stiffness is written as

$$K_{ij} = \sum_{s=1}^{6} \left( \frac{\partial J_{si}}{\partial \zeta^j} t_s - k_s J_{si} J_{sj} \right) - \frac{1}{2} \sum_{k=1}^{3} \sum_{s=1}^{6} \gamma_{ji}^k J_{sk} t_s. \quad (44)$$

Eventually, the matrix form of the stiffness model (44) with the system parameters of the CSJM is given as

$$\boldsymbol{K} = \boldsymbol{D} - \boldsymbol{J}^T \boldsymbol{K}_{\text{diag}} \boldsymbol{J} - \widehat{\boldsymbol{J}^T \boldsymbol{T}}. \quad (45)$$

where $\boldsymbol{D} = \left( \frac{\partial \boldsymbol{J}^T}{\partial \zeta^1} \boldsymbol{T}, \frac{\partial \boldsymbol{J}^T}{\partial \zeta^2} \boldsymbol{T}, \frac{\partial \boldsymbol{J}^T}{\partial \zeta^3} \boldsymbol{T} \right)$ and $\boldsymbol{K}_{\text{diag}} = \text{diag}\{k_1, k_2, \cdots, k_6\}$. It revises the stiffness model of a CDM derived in [26] with additional term of $-\widehat{\boldsymbol{J}^T \boldsymbol{T}}$.

## III. STIFFNESS MODEL IDENTIFICATION

The stiffness model of the CSJM (45) is derived based on the following assumptions: (1) Friction is not taken into account. (2) The links are considered to be rigid. (3) The stiffness of the cables and associate cable driving units are constant. The actual working condition diverges from these assumptions. Moreover, some parameters in (45), such as the cable tensions, the stiffness of the cables and associate cable driving units are difficult to be measured accurately. In this section, a feasible stiffness model identification method is developed, which merely requires to measure the loads applied on the moving-platform of the CSJM and the corresponding displacements.

### A. APPROXIMATION OF THE STIFFNESS MODEL

Considering a static equilibrium pose $\boldsymbol{R}(t)$ of the CSJM with load $\boldsymbol{W}(t) = \begin{pmatrix} \boldsymbol{f}(t) \\ \boldsymbol{\tau}(t) \end{pmatrix}$, and a nearby pose of static equilibrium $\boldsymbol{R}(t + \Delta t)$ with load $\boldsymbol{W}(t + \Delta t)$, the displacement between the two poses is represented by $\Delta \boldsymbol{\zeta}(t) = \boldsymbol{\zeta}(t + \Delta t) - \boldsymbol{\zeta}(t)$, and the increment of the load is represented by $\Delta \boldsymbol{W}(t) = \boldsymbol{W}(t + \Delta t) - \boldsymbol{W}(t)$. According to the stiffness model (33), the stiffness of the CSJM at $\boldsymbol{R}(t)$ can be approximated as

$$\begin{aligned} K_{ij} &= \lim_{\Delta t \to 0} \frac{\tau_i(t + \Delta t) - \tau_i(t)}{\omega^j(t) \Delta t} - \frac{1}{2} \sum_{k=1}^{3} \tau_k(t) \gamma_{ji}^k \\ &\approx \frac{\Delta \tau_i(t)}{\Delta \zeta^j(t)} - \frac{1}{2} \sum_{k=1}^{3} \tau_k(t) \gamma_{ji}^k, \end{aligned} \quad (46)$$

where $\omega^j(t) = \dot{\zeta}^j(t)$ and $\Delta \tau_i(t) = \tau_i(t + \Delta t) - \tau_i(t)$. Consequently, the stiffness $\boldsymbol{K}$ can be computed from (46) when the loads and poses of the CSJM are measured. In this work, the poses are measured by a high precision laser tracker and the loads are measured by a force/torque sensor mounted at the top of the moving-platform. The approximation of the stiffness shown in (46) can be improved when many measurements are performed for different neighboring poses $\boldsymbol{R}(t + \Delta t)$ around $\boldsymbol{R}(t)$.

The matrix form of the stiffness model (33) can be decomposed into two parts

$$\boldsymbol{K} = \boldsymbol{K}_D + \boldsymbol{K}_L, \quad (47)$$

$$ {}^{L}\boldsymbol{P}_{H} = \begin{pmatrix} {}^{L}\boldsymbol{p}_{H_1} & {}^{L}\boldsymbol{p}_{H_2} & {}^{L}\boldsymbol{p}_{H_3} & ({}^{L}\boldsymbol{p}_{H_2} - {}^{L}\boldsymbol{p}_{H_1}) \times ({}^{L}\boldsymbol{p}_{H_3} - {}^{L}\boldsymbol{p}_{H_1}) \\ 1 & 1 & 1 & 0 \end{pmatrix}, \tag{52a} $$

$$ {}^{B}\boldsymbol{P}_{H} = \begin{pmatrix} {}^{B}\boldsymbol{p}_{H_1} & {}^{B}\boldsymbol{p}_{H_2} & {}^{B}\boldsymbol{p}_{H_3} & ({}^{B}\boldsymbol{p}_{H_2} - {}^{B}\boldsymbol{p}_{H_1}) \times ({}^{B}\boldsymbol{p}_{H_3} - {}^{B}\boldsymbol{p}_{H_1}) \\ 1 & 1 & 1 & 0 \end{pmatrix}. \tag{52b} $$

where

$$ \boldsymbol{K}_D = \{\boldsymbol{L}_j \circ \tau_i\} \in \mathbb{R}^{3\times 3}, \quad (i, j = 1, 2, 3), \tag{48a} $$

$$ \boldsymbol{K}_L = \{-\frac{1}{2}\sum_{k=1}^{3} \tau_k(t)\gamma_{ji}^{k}\} = -\hat{\boldsymbol{\tau}} \in \mathbb{R}^{3\times 3}, \quad (i, j, k = 1, 2, 3). \tag{48b} $$

Suppose $N$ sets of data $\{\Delta\boldsymbol{\tau}, \Delta\boldsymbol{\zeta}\}$ are obtained from $N$ measurements, denoting $\boldsymbol{\Psi} = \{\Delta\boldsymbol{\tau}_1, \Delta\boldsymbol{\tau}_2, \cdots, \Delta\boldsymbol{\tau}_N\}$ and $\boldsymbol{\Omega} = \{\Delta\boldsymbol{\zeta}_1, \Delta\boldsymbol{\zeta}_2, \cdots, \Delta\boldsymbol{\zeta}_N\}$, then $\boldsymbol{K}_D$ can be estimated by

$$ \boldsymbol{K}_D \approx \boldsymbol{\Psi}\boldsymbol{\Omega}^{+}, \tag{49} $$

where $\boldsymbol{\Omega}^{+}$ represents the pseudo-inverse of $\boldsymbol{\Omega}$. Thus, the stiffness of the CSJM at pose $\boldsymbol{R}(t)$ can be estimated from $N$ measurements by

$$ \boldsymbol{K} = \boldsymbol{K}_D + \boldsymbol{K}_L \approx \boldsymbol{\Psi}\boldsymbol{\Omega}^{+} - \hat{\boldsymbol{\tau}}(t). \tag{50} $$

### B. IDENTIFICATION PROCEDURES

The procedure of the stiffness identification mainly contains three parts: measurement of the pose of the CSJM, measurement of the load of the CSJM and data processing based on stiffness identification algorithm.

#### 1) MEASUREMENT OF THE POSE OF CSJM

For the CSJM, the pose of the moving frame {A} is measured directly by a laser tracker, which is denoted as ${}^{L}_{A}\boldsymbol{T}$ with respect to the Laser Tracker frame {L}. While the pose of the base frame {B} is measured through three points on the base. The three points are denoted as $H_1$, $H_2$ and $H_3$. In the base frame {B}, the position vectors of the three points are given by ${}^{B}\boldsymbol{p}_{H_1}, {}^{B}\boldsymbol{p}_{H_2}, {}^{B}\boldsymbol{p}_{H_3} \in \mathbb{R}^{3\times 1}$. In the Laser Tracker frame {L}, their position vectors are measured by the laser tracker with a ball reflector, denoted as ${}^{L}\boldsymbol{p}_{H_1}, {}^{L}\boldsymbol{p}_{H_2}, {}^{L}\boldsymbol{p}_{H_3} \in \mathbb{R}^{3\times 1}$. The pose of the base with respect to the Laser Tracker frame {L}, ${}^{L}_{B}\boldsymbol{T}$, satisfies

$$ {}^{L}\boldsymbol{P}_{H} = {}^{L}_{B}\boldsymbol{T}\,{}^{B}\boldsymbol{P}_{H}, \tag{51} $$

where (52a) and (52b), as shown at the top of this page. Then ${}^{L}_{B}\boldsymbol{T}$ can be computed from (51).

Let ${}^{B}_{A}\boldsymbol{T}$ be the pose of moving frame {A} with respect to the base frame {B}, it yields

$$ {}^{B}_{A}\boldsymbol{T} = {}^{L}_{B}\boldsymbol{T}^{-1}\,{}^{L}_{A}\boldsymbol{T}. \tag{53} $$

As

$$ {}^{B}_{A}\boldsymbol{T} = \begin{pmatrix} {}^{B}_{A}\boldsymbol{R} & {}^{B}_{A}\boldsymbol{p} \\ \boldsymbol{0} & 1 \end{pmatrix}, \tag{54} $$

and the origins of two frames {A} and {B} are coincident with each other, i.e., ${}^{B}_{A}\boldsymbol{p} = \boldsymbol{0}$, the pose of the frame {A} with respect to the frame {B} can be described by ${}^{B}_{A}\boldsymbol{R}$.

#### 2) MEASUREMENT OF THE LOAD OF CSJM

The load applied on the moving-platform, $\boldsymbol{W}$, consists of two parts, i.e., the external load applied on the end of moving-platform, $\boldsymbol{W}_E$, and the load generated by the gravity of the moving-platform, $\boldsymbol{W}_G$. They satisfy $\boldsymbol{W} = \boldsymbol{W}_E + \boldsymbol{W}_G$. $\boldsymbol{W}_E$ described in the force/torque sensor frame {S} is denoted as ${}^{S}\boldsymbol{W}_E$, which is measured by the force/torque sensor directly. $\boldsymbol{W}_E$ described in the moving frame {A} is denoted as ${}^{A}\boldsymbol{W}_E$. They have the following relationship

$$ {}^{A}\boldsymbol{W}_E = \mathrm{Ad}^{T}_{{}^{S}_{A}\boldsymbol{T}}\,{}^{S}\boldsymbol{W}_E, \tag{55} $$

where ${}^{S}_{A}\boldsymbol{T}$ represents the pose of the moving frame {A} with respect to the sensor frame {S}, and $\mathrm{Ad}_{{}^{S}_{A}\boldsymbol{T}}$ is the Adjoint Representation of ${}^{S}_{A}\boldsymbol{T}$.

The gravity of the moving-platform, including the weight of the force/torque sensor, denoted as $\boldsymbol{G}$, is applied on a point denoted by a position vector $\boldsymbol{r}_G$, as shown in Figure 1. The gravity generates a load, $\boldsymbol{W}_G$, with respect to the spherical joint. Denoting ${}^{A}\boldsymbol{W}_G$ and ${}^{B}\boldsymbol{W}_G$ as the values of $\boldsymbol{W}_G$ in the moving frame {A} and the base frame {B}, respectively. Similarly, we have

$$ {}^{A}\boldsymbol{W}_G = \mathrm{Ad}^{T}_{{}^{S}_{A}\boldsymbol{T}}\,{}^{B}\boldsymbol{W}_G\,. \tag{56} $$

The corresponding total torque applied on the moving-platform satisfies ${}^{A}\tau = {}^{A}\tau_E + {}^{A}\tau_G$.

#### 3) DATA PROCESSING

For a given pose of CSJM, when the load and pose are measured, the stiffness can be computed via (50). According to (49), at least three measurements are required for computing the stiffness.

## IV. EXPERIMENT

### A. DESCRIPTION OF TESTBED SETUP

In order to validate the proposed stiffness identification method by experiment, an experimental testbed is built, as shown in Figure 3, and the prototype of the CSJM is zoomed in as shown in Figure 4. The key elements of the experimental setup are a prototype of the CSJM, a laser tracker, a force/torque sensor, computers for data acquisition, and counterweights for applying load to the moving-platform. For the moving-platform, $A_2A_3 = A_4A_5 = A_6A_1 = 0.095$m, and $A_1A_2 = A_3A_4 = A_5A_6 = 0.010$m, while

**TABLE 1.** Performance parameters of the laser tracker.

| | Horizontal | Vertical | Distance |
|---|---|---|---|
| Measurement ranges | 360° | ±45° | 40 m |
| Measurement uncertainty (relate to the distance between the laser tracker and the measured point) | ±15 $\mu$m + 6 $\mu$m/m | | |

**TABLE 2.** Performance parameters of the force/torque sensor at temperature 22.2°C ± 1.1°C.

| | $f_x$ | $f_y$ | $f_z$ | $\tau_x$ | $\tau_y$ | $\tau_z$ |
|---|---|---|---|---|---|---|
| Measurement ranges | ±145 N | ±145 N | ±290 N | ±5 Nm | ±5 Nm | ±5 Nm |
| Measurement uncertainty (95% confidence level, percent of full-scale load) | 1.25% | 1.00% | 0.75% | 1.25% | 1.50% | 1.25% |

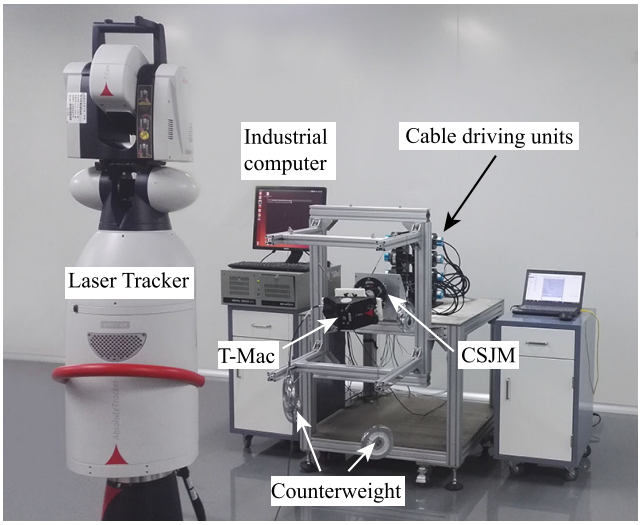


**FIGURE 3.** Experimental testbed for the stiffness identification.

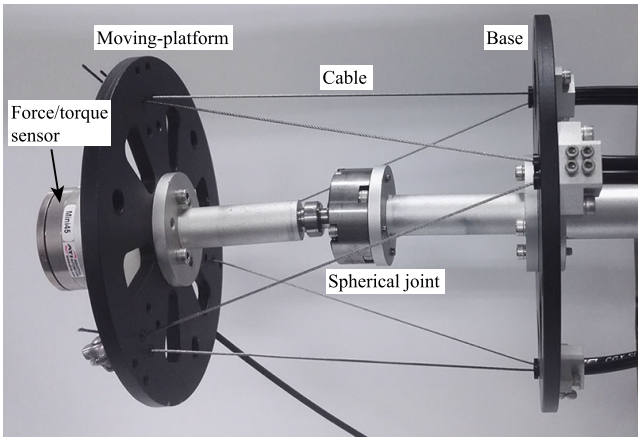


**FIGURE 4.** Prototype of the CSJM.

for the base, $B_1\ B_2 = B_3\ B_4 = B_5\ B_6 = 0.128$m and $B_2\ B_3 = B_4\ B_5 = B_6\ B_1 = 0.005$m. Besides, $OO_A = 0.08$m and $OO_B = 0.08$m. The gravity of the moving-platform $G = \|\boldsymbol{G}\| = 4.82$N, and ${}^A\boldsymbol{r}_G = (0, 0, 0.081)^T$m. In this experiment, the performance parameters of the laser tracker and the force/torque sensor are listed in Table 1 and Table 2, respectively.

### B. EXPERIMENT OF STIFFNESS IDENTIFICATION

In this experiment, the initial pose of the CSJM is $\boldsymbol{R}_0$, and the moment load at $\boldsymbol{R}_0$ described in frame {A} is ${}^A\tau_0$. In order to minimize the effects of measurement noise, 85 measurements are conducted with different loads and different displacements. The influence of the number of measurements for the stiffness identification is revealed in Figure 5, where the determinant of the stiffness det($\boldsymbol{K}$) is employed to evaluate $\boldsymbol{K}$. det($\boldsymbol{K}$) tends to converge as the number of measurements increases, since the increasing number of measurements reduces the effect of the measurement noise. According to (50), the stiffness $\boldsymbol{K}$ is obtained based on the 85 measurement data of poses and loads. The result is summarized in Table 3 and it shows the stiffness $\boldsymbol{K}$ is approximately symmetric as indicated in (37).

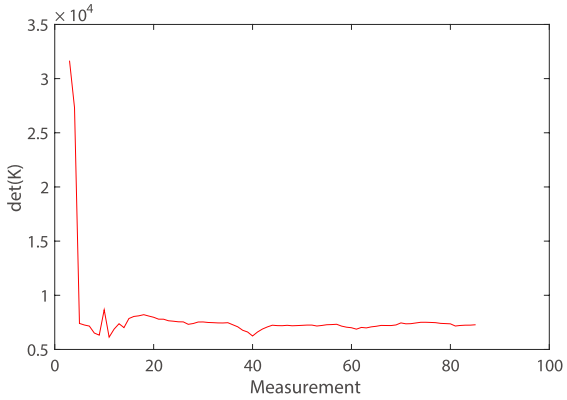


**FIGURE 5.** Curve between measurement and determinant of stiffness $\boldsymbol{K}$.

### C. VERIFICATION OF IDENTIFIED STIFFNESS

If the stiffness of the CSJM is identified, the displacement of the CSJM can be estimated by a known increment of the load. Subsequently, we compare the estimated and actual poses of the CSJM to verify the accuracy of the identified stiffness. In this experiment, additional 5 measurements are conducted to verify the accuracy of the identified stiffness model. The result is summarized in Table 4. The procedure of the verification is illustrated in detail as below.

#### 1) TO APPLY THE LOAD AND MEASURE THE ACTUAL POSE

When we apply a known load (cotangent vector) $\boldsymbol{F}(t) \in \mathbb{R}^3$ on the CSJM, the CSJM will move to a nearby pose $\boldsymbol{R}$. According to (21), the covariant derivative of the applied load $\boldsymbol{F}(t)$ with respect to the displacement $\boldsymbol{V}\Delta t$ is approximated by

$$\nabla_{\boldsymbol{V}\Delta t}\boldsymbol{F}(t) \approx \boldsymbol{K}\Delta\boldsymbol{\zeta}(t). \tag{57}$$

**TABLE 3.** Stiffness identification result at pose $\boldsymbol{R}_0$ with pre-load ${}^{A}\boldsymbol{\tau}_0$.

| Original pose $\boldsymbol{R}_0$ | Pre-load ${}^{A}\boldsymbol{\tau}_0$ (Nm) | $\boldsymbol{K}_D$ | $\boldsymbol{K}_L$ | Stiffness $\boldsymbol{K}_{\text{meas}} = \boldsymbol{K}_D + \boldsymbol{K}_L$ |
|---|---|---|---|---|
| $\begin{pmatrix} 0.992 & -0.060 & -0.111 \\ 0.090 & 0.952 & 0.292 \\ 0.088 & 0.300 & 0.950 \end{pmatrix}$ | $\begin{pmatrix} -0.06 \\ -3.08 \\ 1.07 \end{pmatrix}$ | $\begin{pmatrix} 29.39 & 0.75 & 1.67 \\ -2.53 & 29.96 & -1.07 \\ -4.49 & -1.42 & 6.99 \end{pmatrix}$ | $\begin{pmatrix} 0 & 1.07 & 3.08 \\ -1.067 & 0 & -0.06 \\ -3.08 & 0.06 & 0 \end{pmatrix}$ | $\begin{pmatrix} 29.39 & 1.82 & 4.75 \\ -3.60 & 29.96 & -1.14 \\ -7.57 & -1.35 & 6.99 \end{pmatrix}$ |

**TABLE 4.** Stiffness verification result for the stiffness identification at pose $\boldsymbol{R}_0$ with pre-load ${}^{A}\boldsymbol{\tau}_0$.

| | Col. A<br>Increment of load $\Delta{}^{A}\boldsymbol{\tau}$ (Nm) | Col. B<br>Actual pose $\boldsymbol{R}_{\text{act}}$ | Col. C<br>Estimated pose $\boldsymbol{R}_{\text{est}}$ | Col. D<br>Estimation error $E_\theta$ |
|---|---|---|---|---|
| Case 1 | $\begin{pmatrix} 2.71 \\ -0.93 \\ 0.74 \end{pmatrix}$ | $\begin{pmatrix} 0.961 & -0.255 & -0.104 \\ 0.273 & 0.930 & 0.246 \\ 0.034 & -0.265 & 0.964 \end{pmatrix}$ | $\begin{pmatrix} 0.968 & -0.223 & -0.117 \\ 0.244 & 0.947 & 0.209 \\ 0.064 & -0.231 & 0.971 \end{pmatrix}$ | 0.016 |
| Case 2 | $\begin{pmatrix} 1.94 \\ -0.80 \\ 0.65 \end{pmatrix}$ | $\begin{pmatrix} 0.984 & -0.151 & -0.091 \\ 0.169 & 0.954 & 0.246 \\ 0.050 & -0.257 & 0.965 \end{pmatrix}$ | $\begin{pmatrix} 0.974 & -0.192 & -0.120 \\ 0.216 & 0.948 & 0.233 \\ 0.069 & -0.253 & 0.965 \end{pmatrix}$ | 0.034 |
| Case 3 | $\begin{pmatrix} 2.85 \\ -1.16 \\ 0.68 \end{pmatrix}$ | $\begin{pmatrix} 0.968 & -0.220 & -0.122 \\ 0.243 & 0.940 & 0.239 \\ 0.062 & -0.261 & 0.963 \end{pmatrix}$ | $\begin{pmatrix} 0.968 & -0.217 & -0.124 \\ 0.238 & 0.950 & 0.202 \\ 0.073 & -0.225 & 0.971 \end{pmatrix}$ | 0.023 |
| Case 4 | $\begin{pmatrix} 1.80 \\ -1.45 \\ 0.58 \end{pmatrix}$ | $\begin{pmatrix} 0.977 & -0.152 & -0.152 \\ 0.189 & 0.945 & 0.266 \\ 0.103 & -0.288 & 0.952 \end{pmatrix}$ | $\begin{pmatrix} 0.974 & -0.176 & -0.143 \\ 0.206 & 0.951 & 0.233 \\ 0.095 & -0.256 & 0.962 \end{pmatrix}$ | 0.058 |
| Case 5 | $\begin{pmatrix} 2.34 \\ -1.40 \\ 0.54 \end{pmatrix}$ | $\begin{pmatrix} 0.971 & -0.216 & -0.104 \\ 0.234 & 0.948 & 0.214 \\ 0.052 & -0.232 & 0.971 \end{pmatrix}$ | $\begin{pmatrix} 0.973 & -0.185 & -0.137 \\ 0.211 & 0.953 & 0.216 \\ 0.091 & -0.239 & 0.967 \end{pmatrix}$ | 0.046 |

In addition, $\nabla_{V\Delta t}\boldsymbol{F}$ yields

$$\begin{aligned}\nabla_{V\Delta t}\boldsymbol{F} &= \Delta t \nabla_{\boldsymbol{V}}\boldsymbol{F} \\ &= \Delta t \lim_{\Delta t \to t_0} \frac{\boldsymbol{F}(t+\Delta t) - \boldsymbol{F}(t)}{\Delta t} \\ &\approx \boldsymbol{F}(t+\Delta t) - \boldsymbol{F}(t) \\ &= \Delta \boldsymbol{F}(t). \end{aligned} \tag{58}$$

According to (14), the cotangent vector is left invariant, which means the coordinate of $\boldsymbol{F}(t)$ equals to that of $\boldsymbol{\tau}(t)$, so it yields

$$\Delta \boldsymbol{F}(t) = \Delta \boldsymbol{\tau}(t). \tag{59}$$

Thus, the increment of the applied loads are measured by the force/torque sensor, which are shown in Col. A of Table 4. The actual poses of the CSJM, $\boldsymbol{R}_{\text{act}}$, under the applied loads are measured by the Laser Tracker, which are shown in Col. B of Table 4.

#### 2) TO ESTIMATE THE POSE BY THE STIFFNESS MODEL

Substitute (58) and (59) into (57), it yields

$$\Delta \boldsymbol{\tau}(t) \approx \boldsymbol{K} \Delta \boldsymbol{\zeta}(t). \tag{60}$$

Subsequently, the displacement of the moving-platform is estimated by the identified stiffness $\boldsymbol{K}$ and the known increment of load $\Delta\boldsymbol{\tau}$ as following, where the estimated displacement is represented by $\Delta\boldsymbol{\zeta}_{\text{est}}$,

$$\Delta \boldsymbol{\zeta}_{\text{est}} = \boldsymbol{K}^{-1} \Delta \boldsymbol{\tau}. \tag{61}$$

Consequently, the estimated pose $\boldsymbol{R}_{\text{est}}$ is computed by

$$\boldsymbol{R}_{\text{est}} = \boldsymbol{R}_0 e^{\Delta \hat{\boldsymbol{\xi}}_{\text{est}}}, \tag{62}$$

and the result is summarized in Col. C of Table 4.

#### 3) TO EVALUATE THE ESTIMATION ERROR

The difference (or error) between the estimated pose $\boldsymbol{R}_{\text{est}}$ and the actual pose $\boldsymbol{R}_{\text{act}}$ can be represented by a matrix $\boldsymbol{R}_{\text{err}} \in SO(3)$, which satisfies

$$\boldsymbol{R}_{\text{err}} = \boldsymbol{R}_{\text{act}}^{-1} \boldsymbol{R}_{\text{est}} = e^{\hat{\boldsymbol{\xi}}_{\text{err}}}. \tag{63}$$

According to the log function on $SO(3)$ [27], we have

$$\hat{\boldsymbol{\xi}}_{\text{err}} = \log \boldsymbol{R}_{\text{err}}. \tag{64}$$

Then, we define a scalar $E_\theta$, named estimation error, to represent the difference between the estimated pose $\boldsymbol{R}_{\text{est}}$ and the actual pose $\boldsymbol{R}_{\text{act}}$ to evaluate the accuracy of the proposed stiffness model. The definition of the estimation error $E_\theta$ is given below

$$E_\theta = \|\boldsymbol{\zeta}_{\text{err}}\|. \tag{65}$$

The result is summarized in Col. D of Table 4. The small differences between the estimated poses and the actual poses show that the proposed stiffness identification method is effective for the CSJM.

### D. DISCUSSION

As shown in Table 3, the stiffness matrix of the CSJM, $\boldsymbol{K}$, is not exactly symmetric. And as shown in Table 4, there are differences between the estimated poses and actual poses. The major factors that affect the accuracy of the stiffness identification are summarized as following:

- Effect of the friction. When the load applied on the CSJM during stiffness identification, the frictions between the cables and the holes on the base, the cables

and their outer housing affect the deformation of the cables and cable driving units. This factor can be reduced by improving the design and fabrication of the CSJM.

- Noise of the measurement. The measurement procedure and the precision of equipments (such as the force/torque sensor and the laser tracker) also affect the accuracy of the stiffness identification. This factor can be reduced by using high precision equipments and performing many measurements.
- Algorithm of the stiffness identification. The algorithm of the stiffness identification is based on the approximation of the covariant derivative, which causes the systematical error.

## V. CONCLUSION

In this paper, an enhanced stiffness model and associate identification method are developed on $SO(3)$ for a low-stiffness CSJM. Since the trajectory of the CSJM is a curve on $SO(3)$, its instantaneous displacement and exerted load can be represented by the vectors on the tangent and cotangent spaces of $SO(3)$, respectively. As we cannot perform the algebraic operations between vectors on different tangent or cotangent spaces, a Riemannian metric is defined on $SO(3)$ to evaluate the lengths of vectors and the angles between vectors, and the Levi-Civita connection is introduced into $SO(3)$ to bridge different vector spaces. Subsequently, the stiffness of the CSJM is derived by the covariant derivative of the load with respect to the displacement. The derived stiffness matrix is proved to be symmetric for a conservative mechanical system. In order to reveal the relationship between the stiffness and the system parameters of the CSJM, the stiffness matrix represented by the system parameters is derived based on the kinetostatics of the CSJM. It shows that the stiffness of the CSJM is determined by its pose, the stiffness of the cables and the associate cable driving units, and the cable tensions. As some of these parameters cannot be measured accurately, an alternative stiffness identification method is developed. It is based on the approximation of the covariant derivative of the load with respect to the displacement, which only requires to measure the loads and displacements of the CSJM. Eventually, the identification procedure is proposed and the experiment is conducted on the testbed. The results show that the stiffness model and associate identification method are effective for the CSJM, and they can be extended to other low-stiffness robotic manipulators.

## REFERENCES

[1] T. Dallej, M. Gouttefarde, N. Andreff, M. Michelin, and P. Martinet, "Towards vision-based control of cable-driven parallel robots," in *Proc. IEEE/RSJ Int. Conf. Intell. Robots Syst. (IROS)*, Sep. 2011, pp. 2855–2860.

[2] R. de Rijk, M. Rushton, and A. Khajepour, "Out-of-plane vibration control of a planar cable-driven parallel robot," *IEEE/ASME Trans. Mechatronics*, vol. 23, no. 4, pp. 1684–1692, Aug. 2018.

[3] S. Qian, B. Zi, D. Wang, and Y. Li, "Development of modular cable-driven parallel robotic systems," *IEEE Access*, vol. 7, pp. 5541–5553, 2019.

[4] Y. Wang, C. Song, T. Zheng, D. Lau, K. Yang, and G. Yang, "Cable routing design and performance evaluation for multi-link cable-driven robots with minimal number of actuating cables," *IEEE Access*, to be published.

[5] X. Dong, D. Axinte, D. Palmer, S. Cobos, M. Raffles, A. Rabani, and J. Kell, "Development of a slender continuum robotic system for on-wing inspection/repair of gas turbine engines," *Robot. Comput. Integr. Manuf.*, vol. 44, pp. 218–229, Apr. 2017.

[6] M. Wang, D. Palmer, X. Dong, D. Alatorre, D. Axinte, and A. Norton, "Design and development of a slender dual-structure continuum robot for *in-situ* aeroengine repair," in *Proc. IEEE/RSJ Int. Conf. Intell. Robots Syst. (IROS)*, Oct. 2018, pp. 5648–5653.

[7] D. Axinte, X. Dong, D. Palmer, A. Rushworth, S. C. Guzman, A. Olarra, I. Arizaga, E. Gomez-Acedo, K. Txoperena, K. Pfeiffer, F. Messmer, M. Gruhler, and J. Kell, "MiRoR–miniaturized robotic systems for holistic *in-situ* repair and maintenance works in restrained and hazardous environments," *IEEE/ASME Trans. Mechatronics*, vol. 23, no. 2, pp. 978–981, Apr. 2018.

[8] P. Dion-Gauvin and C. Gosselin, "Dynamic point-to-point trajectory planning of a three-DOF cable-suspended mechanism using the hypocycloid curve," *IEEE/ASME Trans. Mechatronics*, vol. 23, no. 4, pp. 1964–1972, Aug. 2018.

[9] D. Song, L. Zhang, and F. Xue, "Configuration optimization and a tension distribution algorithm for cable-driven parallel robots," *IEEE Access*, vol. 6, pp. 33928–33940, 2018.

[10] H. Wang, J. Kinugawa, and K. Kosuge, "Exact kinematic modeling and identification of reconfigurable cable-driven robots with dual-pulley cable guiding mechanisms," *IEEE/ASME Trans. Mechatronics*, vol. 24, no. 2, pp. 774–784, Apr. 2019.

[11] Y. Xia, K. Xu, Y. Li, G. Xu, and X. Xiang, "Adaptive trajectory tracking control of a cable-driven underwater vehicle on a tension leg platform," *IEEE Access*, vol. 7, pp. 35512–35531, 2019.

[12] S. K. Mustafa, G. Yang, S. H. Yeo, and W. Lin, "Optimal design of a bio-inspired anthropocentric shoulder rehabilitator," *Appl. Bionics Biomech.*, vol. 3, no. 3, pp. 199–208, 2006.

[13] L. Zhang, L. Li, Y. Zou, K. Wang, X. Jiang, and H. Ju, "Force control strategy and bench press experimental research of a cable driven astronaut rehabilitative training robot," *IEEE Access*, vol. 5, pp. 9981–9989, 2017.

[14] J.-Y. Kuan, K. A. Pasch, and H. M. Herr, "A high-performance cable-drive module for the development of wearable devices," *IEEE/ASME Trans. Mechatronics*, vol. 23, no. 3, pp. 1238–1248, Jun. 2018.

[15] Y. Zou, N. Wang, X. Wang, H. Ma, and K. Liu, "Design and experimental research of movable cable-driven lower limb rehabilitation robot," *IEEE Access*, vol. 7, pp. 2315–2326, 2019.

[16] A. Klimchik, D. Chablat, and A. Pashkevich, "Stiffness modeling for perfect and non-perfect parallel manipulators under internal and external loadings," *Mech. Mach. Theory*, vol. 79, pp. 1–28, Sep. 2014.

[17] C. Dumas, S. Caro, M. Cherif, S. Garnier, and B. Furet, "Joint stiffness identification of industrial serial robots," *Robotica*, vol. 30, no. 4, pp. 649–659, 2012.

[18] H. Jamshidifar, A. Khajepour, B. Fidan, and M. Rushton, "Kinematically-constrained redundant cable-driven parallel robots: Modeling, redundancy analysis, and stiffness optimization," *IEEE/ASME Trans. Mechatronics*, vol. 22, no. 2, pp. 921–930, Apr. 2017.

[19] K. Yang, G. Yang, J. Wang, T. Zheng, and W. Yang, "Design analysis of a 3-DOF cable-driven variable-stiffness joint module," in *Proc. IEEE Int. Conf. Robot. Biomimetics (ROBIO)*, Dec. 2016, pp. 529–534.

[20] J. K. Salisbury, "Active stiffness control of a manipulator in Cartesian coordinates," in *Proc. IEEE Conf. Decis. Control*, Dec. 1980, pp. 95–100.

[21] C. Gosselin, "Stiffness mapping for parallel manipulator," *IEEE Trans. Robot. Autom.*, vol. 6, no. 3, pp. 377–382, Jun. 1990.

[22] M. Griffis and J. Duffy, "Global stiffness modeling of a class of simple compliant couplings," *Mech. Mach. Theory*, vol. 28, no. 2, pp. 207–224, 1993.

[23] N. Ciblak and H. Lipkin, "Asymmetric cartesian stiffness for the modelling of compliant robotic systems," *Robot., Kinematics, Dyn. Controls*, vol. 72, pp. 197–204, Jan. 1994.

[24] S.-F. Chen and I. Kao, "Conservative congruence transformation for joint and Cartesian stiffness matrices of robotic hands and fingers," *Int. J. Robot. Res.*, vol. 19, no. 9, pp. 835–847, 2000.

[25] S.-F. Chen, "The spatial conservative congruence transformation for manipulator stiffness modeling with coordinate and noncoordinate bases," *J. Robot. Syst.*, vol. 22, no. 1, pp. 31–44, 2005.

[26] W. B. Lim, S. H. Yeo, G. Yang, and I.-M. Chen, "Design and analysis of a cable-driven manipulator with variable stiffness," in *Proc. IEEE Int. Conf. Robot. Autom. (ICRA)*, May 2013, pp. 4519–4524.

[27] R. N. Murray, Z. Li, and S. Sastry, *A Mathematical Introduction to Robotic Manipulation*. Boca Raton, FL, USA: CRC Press, 1994.

[28] L. W. Tu, *An Introduction to Manifolds*. New York, NY, USA: Springer, 2011.
[29] M. Zefran and R. V. Kumar, "A geometric approach to the study of the Cartesian stiffness matrix," *J. Mech. Des.*, vol. 124, no. 1, pp. 30–38, 2002.
[30] C. Domenico, "Cartesian stiffness for wrist joints: Analysis on the lie group of 3d rotations and geometric approximation for experimental evaluation," *Comput. Methods Biomechanics Biomed. Eng.*, vol. 16, no. 9, pp. 975–986, 2013.
[31] W. Khalil and E. Dombre, *Modeling, Identification and Control of Robots*. New York, NY, USA: Taylor & Francis, 2004.
[32] Z. Jinjuan, W. Shijun, M. Jingzhi, and G. Pu, "An identification method of stiffness of mechanical joint," in *Proc. IEEE Int. Conf. Consum. Electron.*, Apr. 2011, pp. 3925–3928.
[33] G. Alici and B. Shirinzadeh, "Enhanced stiffness modeling, identification and characterization for robot manipulators," *IEEE Trans. Robot.*, vol. 21, no. 4, pp. 554–564, Aug. 2005.
[34] A. Jubien, G. Abba, and M. Gautier, "Joint stiffness identification of a heavy kuka robot with a low-cost clamped end-effector procedure," in *Proc. IEEE 11th Int. Conf. Inform. Control, Autom. Robot.*, Sep. 2014, pp. 585–591.
[35] A. Janot, P.-O. Vandanjon, and M. Gautier, "A generic instrumental variable approach for industrial robot identification," *IEEE Trans. Control Syst. Technol.*, vol. 22, no. 1, pp. 132–145, Jan. 2014.
[36] J. Wua, J. Wanga, and Z. You, "An overview of dynamic parameter identification of robots," *Robot. Comput. Integr. Manuf.*, vol. 26, no. 5, pp. 414–419, 2010.
[37] J. Swevers, W. Verdonck, and J. D. Schutter, "Dynamic model identification for industrial robots," *IEEE Control Syst.*, vol. 27, no. 5, pp. 58–71, Oct. 2007.
[38] K. R. Kozlowski, *Modelling and Identification in Robotics*. London, U.K.: Springer, 2008.
[39] M. Östring, S. Gunnarsson, and M. Norrlöf, "Closed-loop identification of an industrial robot containing flexibilities," *Control Eng. Pract.*, vol. 11, no. 3, pp. 291–300, 2003.
[40] M. Gautier, A. Jubien, A. Janot, and P.-P. Robet, "Dynamic identification of flexible joint manipulators with an efficient closed loop output error method based on motor torque output data," in *Proc. IEEE Int. Conf. Robot. Autom. (ICRA)*, May 2013, pp. 2949–2955.
[41] C. Dumas, S. Caro, S. Garnier, and B. Furet, "Joint stiffness identification of six-revolute industrial serial robots," *Robot. Comput.-Integr. Manuf.*, vol. 27, no. 4, pp. 881–888, 2011.
[42] G. Yang, W. Lin, M. S. Kurbanhusen, P. C. Bang, and S. H. Yeo, "Kinematic design of a 7-DOF cable-driven humanoid arm: A solution-in-nature approach," in *Proc. IEEE/ASME Int. Conf. Adv. Intell. Mechatronics (AIM)*, Jul. 2005, pp. 24–28.
[43] J. M. Lee, *Introduction to Riemannian Manifolds*. Springer, 2018.
[44] B. F. Schutz, *Geometrical Methods of Mathematical Physics*. Cambridge, U.K.: Cambridge Univ. Press, 1980.

**KAISHENG YANG** received the B.Eng. degree in mechanical engineering from the Zhejiang University of Technology, China, in 2008, and the M.Eng. degree from Zhejiang University, China, in 2011. He is currently pursuing the Ph.D. degree with the University of Chinese Academy of Sciences, China.

From 2011 to 2013, he was a Mechatronics Engineer in several companies. Since 2013, he has been a Researcher in robotics and automation with Zhejiang Marine Development Research Institute, China. His research interests include cable-driven manipulators, bionic robots, and mechatronics systems. He is also serving as a Technical Reviewer for *Advances in Mechanical Engineering*.

**GUILIN YANG** received the B.Eng. and M.Eng. degrees from the Jilin University of Technology, China, in 1985 and 1988, respectively, and the Ph.D. degree from Nanyang Technological University, Singapore, in 1999.

From 1998 to 2013, he was a Scientist, a Senior Scientist, and the Manager of the Mechatronics Group, Singapore Institute of Manufacturing Technology, Singapore. Since 1988, he has been a Lecturer, the Division Head, and the Vice Dean of the School of Mechanical Engineering, Shijiazhuang Railway Institute, China. He joined the Ningbo Institute of Material Technology and Engineering, Chinese Academy of Sciences, China, in 2013, where he is also a Professor and the Vice-President. He has published over 280 technical articles in referred journals and conferences. His current research interests include precision actuators, parallel-kinematics machines, modular robots, cable-driven manipulators, and industrial robots. He is also an Associate Editor of IEEE ACCESS.

**SI-LU CHEN** received the B.Eng. and Ph.D. degrees in electrical engineering from the National University of Singapore (NUS), in 2005 and 2010, respectively.

From 2010 to 2011, he was a Senior Engineer on motion control with Manufacturing Integration Technology Ltd., a Singapore-based semiconductor machine designer. From 2011 to 2017, he was a Scientist with the Mechatronics Group, Singapore Institute of Manufacturing Technology (SIMTech), Agency for Science Technology and Research (A*STAR). During that period, he also acted as a Co-PI of the SIMTech-NUS Joint Lab on Precision Motion Systems, an Adjunct Assistant Professor of NUS, and a Ph.D. Co-Advisor for the A*STAR Graduate School. Since 2017, he has been a Professor with the Ningbo Institute of Industrial Technology, Chinese Academy of Sciences. His current research interests include design and optimization of high-speed motion control systems and beyond-rigid-body control for compliant light-weight systems. He is currently serving as a Technical Reviewer for the IEEE/ASME TRANSACTIONS OF MECHATRONICS, *Journal of Mechatronics* (IFAC), and *ISA Transactions*.

**YI WANG** received the B.Eng. degree from Southwest Jiaotong University, China, in 2015. He is currently pursuing the Ph.D. degree with the University of Chinese Academy of Sciences, China. His research interests include cable-driven robots and mechanical design.

**WENJUN SHEN** received the B.Eng. degree from the China University of Geosciences, Wuhan, China, in 2017. She is currently pursuing the Ph.D. degree with the University of Chinese Academy of Sciences, China. Her research interest includes cable-driven continuum robots.

**TIANJIANG ZHENG** received the B.Eng. degree in automation and the M.Eng. degree in control theory and control engineering from Shenyang Ligong University, Shenyang, China, in 2006 and 2009, respectively, and the Ph.D. degree in robotics, cognition and interaction technology from the University of Genoa, Italy, in 2013.

From 2013 to 2015, he was a Research Assistant with the Precision Drive and Advanced Robot Group, Ningbo Institute of Materials Technology and Engineering, Chinese Academy of Sciences, China, where he has been a Senior Engineer, since 2016. He has published more than 20 articles and has applied more than ten patents. His research interests include the control of mobile robots, mobile manipulations, continuum manipulations, and parallel robots.

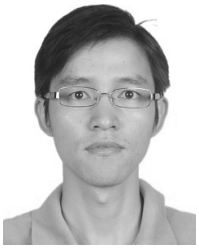

**ZAOJUN FANG** received the B.Eng. degree from the University of Science and Technology Liaoning, China, in 2005, and the M.Eng. and Ph.D. degrees from the Institute of Automation, Chinese Academy of Sciences, China, in 2008 and 2011, respectively.

He is currently a Professor with the Zhejiang Key Laboratory of Robotics and Intelligent Manufacturing Equipment Technology, Ningbo Institute of Materials Technology and Engineering, Chinese Academy of Sciences. His current research interests include robot vision, robot control, and automation.

**CHONGCHONG WANG** received the B.Eng. degree in electronics from Northeast Normal University, China, in 2011, and the Ph.D. degree in optics engineering from the University of Chinese Academy of Sciences, China, in 2016. Since 2016, she has been a Research Assistant with the Ningbo Institute of Industrial Technology, Chinese Academy of Sciences (CAS). Her research interests include the robot dynamic modeling, industrial robots control, and collaborative robots force control.